



The Fierz convergence criterion: a controlled approach to strongly-interacting systems with small embedded clusters

Thomas Ayral, Jaksa Vucicevic, Olivier Parcollet

► To cite this version:

Thomas Ayral, Jaksa Vucicevic, Olivier Parcollet. The Fierz convergence criterion: a controlled approach to strongly-interacting systems with small embedded clusters. 2017. cea-01550535v1

HAL Id: cea-01550535

<https://cea.hal.science/cea-01550535v1>

Preprint submitted on 29 Jun 2017 (v1), last revised 3 Oct 2022 (v2)

HAL is a multi-disciplinary open access archive for the deposit and dissemination of scientific research documents, whether they are published or not. The documents may come from teaching and research institutions in France or abroad, or from public or private research centers.

L'archive ouverte pluridisciplinaire **HAL**, est destinée au dépôt et à la diffusion de documents scientifiques de niveau recherche, publiés ou non, émanant des établissements d'enseignement et de recherche français ou étrangers, des laboratoires publics ou privés.

The Fierz convergence criterion: a controlled approach to strongly-interacting systems with small embedded clusters

Thomas Ayral,^{1,2} Jaksa Vučičević,^{2,3} and Olivier Parcollet²

¹*Physics and Astronomy Department, Rutgers University, Piscataway, NJ 08854, USA*

²*Institut de Physique Théorique (IPhT), CEA, CNRS, UMR 3681, 91191 Gif-sur-Yvette, France*

³*Scientific Computing Laboratory, Center for the Study of Complex Systems, Institute of Physics Belgrade, University of Belgrade, Pregrevica 118, 11080 Belgrade, Serbia*

We present an embedded-cluster method, based on the TRILEX formalism, that turns the Fierz ambiguity, inherent to approaches based on a bosonic decoupling of local fermionic interactions, into a convergence criterion. It is based on the approximation of the three-leg vertex by a coarse-grained vertex computed by solving a self-consistently determined multi-site effective impurity model. The computed self-energies are, by construction, continuous functions of momentum. We show that, in three interaction and doping regimes of parameters of the two-dimensional Hubbard model, these self-energies are very close to numerically exact benchmark results for clusters of size four only. We show that the Fierz parameter, which parametrizes the freedom in the Hubbard-Stratonovich decoupling, can be used as a quality control parameter. By contrast, the $GW +$ extended dynamical mean field theory approximation with four cluster sites is shown to yield good results only in the weak-coupling regime and for a particular decoupling. Finally, we show that the vertex has spatially nonlocal components only at low energy.

Two major approaches have been put forth to fathom the nature of high-temperature superconductivity. Spin fluctuation theory^{1–8}, inspired by the early experiments on cuprate compounds, is based on the introduction of phenomenological bosonic fluctuations coupled to the electrons. It belongs to a larger class of methods, including the fluctuation-exchange (FLEX)⁹ and GW approximations^{10,11}, or the Eliashberg theory of superconductivity¹². In the Hubbard model, these methods can formally be obtained by decoupling the electronic interactions with Hubbard-Stratonovich bosons carrying charge, spin or pairing fluctuations. They are particularly well suited for describing the system’s long-range modes. However, they suffer from two main drawbacks: without an analog of Migdal’s theorem for spin fluctuations, they are quantitatively uncontrolled; worse, the results depend on the precise form of the bosonic fluctuations used to decouple the interaction term, an issue referred to as the “Fierz ambiguity”^{13–18}.

A second class of methods, following Anderson¹⁹, puts primary emphasis on the fact that the undoped compounds are Mott insulators, where local physics plays a central role. Approaches like dynamical mean field theory (DMFT)²⁰ and its cluster extensions^{21–25}, which self-consistently map the lattice problem onto an effective problem describing a cluster of interacting atoms embedded in a noninteracting host, are tools of choice to examine Anderson’s idea. Cluster DMFT has indeed been shown to give a consistent qualitative picture of cuprate physics, including pseudogap and superconducting phases^{26–54}. Compared to fluctuation theories, it *a priori* comes with a control parameter, the size N_c of the embedded cluster. However, this is of limited practical use, since the convergence with N_c is non-

monotonic for small N_c ³³, requiring large N_c ’s, which cannot be reached in interesting physical regimes due to the Monte-Carlo negative sign problem. Thus, converged cluster DMFT results can only be obtained at high temperatures⁵⁵. There, detailed studies^{56–58} point to the importance of (possibly long-ranged) spin fluctuations, calling for a unification of both classes of approaches. First steps in this direction have been accomplished by diagrammatic extensions of DMFT^{59–80}, and by the single-site TRILEX formalism^{81,82}, which interpolates between long-range and Mott physics, and describes aspects of pseudogap physics and the d -wave superconducting dome⁸³.

In this Letter, we turn the Fierz ambiguity into a convergence criterion using the cluster extension of TRILEX. Like fluctuation approaches, it is based on the introduction of bosonic degrees of freedom. Like cluster DMFT, it self-consistently maps the corresponding electron-boson problem onto a cluster impurity problem. The latter is solved for its three-leg vertex, which is used as a cluster vertex correction to the self-energies. This approach remedies the deficiencies of fluctuation approaches by endowing them with a control parameter, thus curing the absence of a Migdal theorem. In some parameter regimes, it can solve the cluster DMFT large- N_c stalemate by instead requiring minimal sensitivity to the Fierz parameter as a convergence criterion of the solution.

To illustrate the method, we focus on the two-dimensional Hubbard model, the simplest model to describe high-temperature superconductors. It is defined

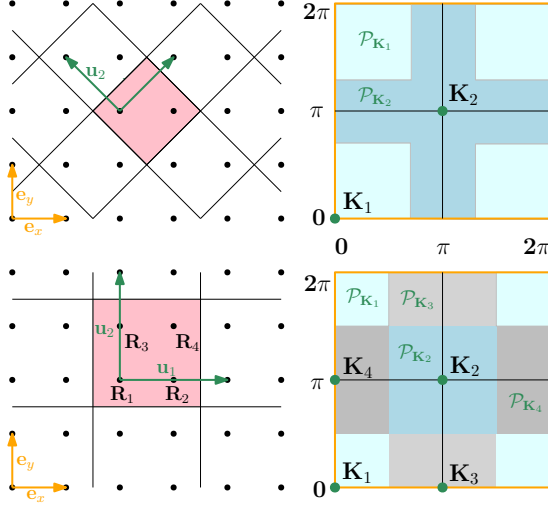


Figure 1. Cluster geometry: real (left) and reciprocal (right) space, for $N_c = 2$ (top) and $N_c = 4$ (bottom). \mathbf{e}_x and \mathbf{e}_y (\mathbf{u}_1 and \mathbf{u}_2) are the unit vectors of the Bravais (super)lattice. The colored patches $\mathcal{P}_{\mathbf{K}_i}$ are of equal area

by the Hamiltonian:

$$H = \sum_{ij\sigma} t_{ij} c_{i\sigma}^\dagger c_{j\sigma} + U \sum_i n_{i\uparrow} n_{i\downarrow} \quad (1)$$

where $c_{i\sigma}^\dagger$ ($c_{i\sigma}$) creates (annihilates) an electron of spin σ at Bravais site \mathbf{r}_i , t_{ij} is the hopping matrix (with [next]-nearest-neighbor hopping parametrized by t [t']), and U the local electronic repulsion.

As in DMFT, there are several ways to extend the TRILEX method to cluster impurity problems. Here, we consider the analog of the dynamical cluster approximation (DCA^{21,22,25}), which uses periodic clusters and hence does not break the translational symmetry of the lattice, at the price of allowing for discontinuities in the momentum dependence of the *vertex function*. Other cluster variants such as a real-space version, inspired from cellular DMFT^{23,24}, are also possible, but break translation invariance and require arbitrary reperiodization procedures.

Cluster TRILEX, like cluster extensions of DMFT, consists in self-consistently mapping the lattice problem defined in Eq. (1) onto an interacting cluster of impurities. We thus straightforwardly generalize the single-site impurity model of TRILEX^{81,82} to a cluster impurity model defined by the action:

$$\begin{aligned} S_{\text{imp}} \equiv & \iint_{\tau\tau'} \sum_{ij\sigma} c_{i\sigma\tau}^* \left\{ -[\mathcal{G}^{-1}]_{ij}(\tau - \tau') \right\} c_{j\sigma\tau'} \\ & + \frac{1}{2} \iint_{\tau\tau'} \sum_{ijI} n_{i\tau}^I \left\{ -[\mathcal{U}^{-1}]_{ij}^I(\tau - \tau') \right\} n_{j\tau'}^I \end{aligned} \quad (2)$$

The latin indices $i, j = 1 \dots N_c$ stand for the cluster positions $\mathbf{R}_i, \mathbf{R}_j$ (shown in Fig. 1 along with the cluster momenta $\{\mathbf{K}_i\}_{i=1\dots N_c}$). $c_{i\sigma\tau}^*$ and $c_{i\sigma\tau}$ are conjugate Grassmann fields, τ denotes imaginary time ($i\omega$ [resp. $i\Omega$] will later denote the corresponding fermionic [resp. bosonic] Matsubara frequencies), and n^I denotes density ($I = 0$) or spin ($I = x, y, z$), i.e. $n_{i\tau}^I \equiv \sum_{\sigma\sigma'} c_{i\sigma\tau}^* \sigma_{\sigma\sigma'}^I c_{i\sigma'\tau}$, where $\sigma_{\sigma\sigma'}^I$ is the 2×2 identity matrix ($I = 0$) or the Pauli matrices ($I = x, y, z$). Due to SU(2) invariance, $\mathcal{U}^x = \mathcal{U}^y = \mathcal{U}^z$: we introduce an index η to distinguish between the charge component $\mathcal{U}^{\eta=\text{ch}} \equiv \mathcal{U}^0$ and the spin components $\mathcal{U}^{\eta=\text{sp}} \equiv \mathcal{U}^x = \mathcal{U}^y = \mathcal{U}^z$.

This cluster impurity model is used to compute the cluster impurity vertex $\Lambda_{\text{imp}}^\eta(\mathbf{K}, \mathbf{Q}; i\omega, i\Omega)$ (all computational details are given in the Suppl. Mat.). Next, in the spirit of DCA, we want to use $\Lambda_{\text{imp}}^\eta(\mathbf{K}, \mathbf{Q}; i\omega, i\Omega)$ to approximate the momentum dependence of the lattice vertex $\Lambda_{\mathbf{k}\mathbf{q}}^\eta(i\omega, i\Omega)$ by a coarse-graining procedure. We recall that DCA consists in coarse-graining the cluster *self-energy* as $\Sigma(\mathbf{k}, i\omega) \approx \sum_{\mathbf{K}} \theta_{\mathbf{K}}(\mathbf{k}) \Sigma_{\text{imp}}(\mathbf{K}, i\omega)$, where $\Sigma_{\text{imp}}(\mathbf{K}, i\omega)$ is the cluster impurity self-energy, and $\theta_{\mathbf{K}}(\mathbf{k}) = 1$ if \mathbf{k} belongs to patch $\mathcal{P}_{\mathbf{K}}$, and vanishes otherwise. For the vertex function, the passage from $\Lambda_{\text{imp}}^\eta(\mathbf{K}, \mathbf{Q}; i\omega, i\Omega)$ to an approximate lattice vertex $\Lambda_{\mathbf{k}, \mathbf{q}}^\eta(i\omega, i\Omega)$ is not as straightforward. There are several possible coarse-grainings for the vertex. We choose the following two, which ensure that a constant vertex is coarse-grained as a constant:

$$\Lambda_{\mathbf{k}\mathbf{q}}^{\eta, \Sigma}(i\omega, i\Omega) \equiv \sum_{\mathbf{K}, \mathbf{Q}} \theta_{\mathbf{K}+\mathbf{Q}}(\mathbf{k} + \mathbf{q}) \theta_{\mathbf{Q}}(\mathbf{q}) \Lambda_{\text{imp}}^\eta(\mathbf{K}, \mathbf{Q}; i\omega, i\Omega) \quad (3a)$$

$$\Lambda_{\mathbf{k}\mathbf{q}}^{\eta, P}(i\omega, i\Omega) \equiv \sum_{\mathbf{K}, \mathbf{Q}} \theta_{\mathbf{K}}(\mathbf{k}) \theta_{\mathbf{K}+\mathbf{Q}}(\mathbf{k} + \mathbf{q}) \Lambda_{\text{imp}}^\eta(\mathbf{K}, \mathbf{Q}; i\omega, i\Omega) \quad (3b)$$

We use it to compute the self-energy $\Sigma(\mathbf{k}, i\omega)$ and polarization $P^\eta(\mathbf{q}, i\Omega)$, given by the exact Hedin expressions:

$$\Sigma(\mathbf{k}, i\omega) = - \sum_{\eta} m_{\eta} \sum_{\mathbf{q}, i\Omega} G_{\mathbf{k}+\mathbf{q}, i\omega+i\Omega} W_{\mathbf{q}, i\Omega}^\eta \Lambda_{\mathbf{k}\mathbf{q}}^\eta(i\omega, i\Omega) \quad (4a)$$

$$P^\eta(\mathbf{q}, i\Omega) = 2 \sum_{\mathbf{k}, i\omega} G_{\mathbf{k}+\mathbf{q}, i\omega+i\Omega} G_{\mathbf{k}, i\omega} \Lambda_{\mathbf{k}\mathbf{q}}^\eta(i\omega, i\Omega) \quad (4b)$$

with $m_{\text{ch}} = 1$ and $m_{\text{sp}} = 3$. Using (3a) (resp. (3b)) for Σ (resp. P), we obtain:

$$\Sigma_{\mathbf{k}}(i\omega) \equiv - \sum_{\eta, \mathbf{K}, \mathbf{Q}} \sum_{\mathbf{q}, i\Omega} m_{\eta} G_{\mathbf{k}+\mathbf{q}, i\omega+i\Omega}^{(\mathbf{K}+\mathbf{Q})} W_{\mathbf{q}, i\Omega}^{\eta, (\mathbf{Q})} \Lambda_{\text{imp}}^\eta(\mathbf{K}\mathbf{Q}; i\omega, i\Omega) \quad (5a)$$

$$P_{\mathbf{q}}^\eta(i\Omega) \equiv 2 \sum_{\mathbf{K}, \mathbf{Q}} \sum_{\mathbf{k}, i\omega} G_{\mathbf{k}+\mathbf{q}, i\omega+i\Omega}^{(\mathbf{K}+\mathbf{Q})} G_{\mathbf{k}, i\omega}^{\mathbf{K}} \Lambda_{\text{imp}}^\eta(\mathbf{K}, \mathbf{Q}; i\omega, i\Omega) \quad (5b)$$

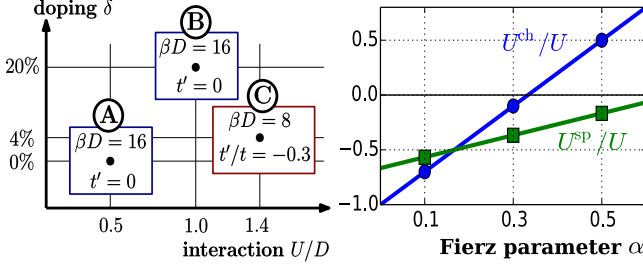


Figure 2. Parameter regimes studied in this work. *Left panel*: points A, B, C (β : inverse temperature, $D = 4t$, δ : doping per site). *Right panel*: U^{ch} and U^{sp} vs. α .

with $X_{\mathbf{k}}^{\mathbf{K}}(i\omega) \equiv \theta_{\mathbf{K}}(\mathbf{k})X(\mathbf{k}, i\omega)$. As convolutions of continuous functions of \mathbf{k} (G and W) with a piecewise-constant function (Λ), Σ and P are continuous in \mathbf{k} by construction.

The (cluster) TRILEX algorithm aims at adjusting the cluster dynamical mean fields $\mathcal{G}_{ij}(\tau)$ and $\mathcal{U}_{ij}^{\eta}(\tau)$ so as to satisfy the self-consistency conditions:

$$G_{\text{imp}}(\mathbf{K}, i\omega)[\mathcal{G}, \mathcal{U}] = G_{\mathbf{K}}(i\omega) \quad (6a)$$

$$W_{\text{imp}}^{\eta}(\mathbf{Q}, i\Omega)[\mathcal{G}, \mathcal{U}] = W_{\mathbf{Q}}^{\eta}(i\Omega) \quad (6b)$$

The left-hand sides are computed by solving the impurity model. The right-hand sides are the patch-averaged lattice Green's functions:

$$G_{\mathbf{K}}(i\omega) \equiv \sum_{\mathbf{k} \in \mathcal{P}_{\mathbf{K}}} G(\mathbf{k}, i\omega) \quad (7a)$$

$$W_{\mathbf{Q}}^{\eta}(i\Omega) \equiv \sum_{\mathbf{q} \in \mathcal{P}_{\mathbf{Q}}} W^{\eta}(\mathbf{q}, i\Omega) \quad (7b)$$

$G(\mathbf{k}, i\omega)$ and $W(\mathbf{q}, i\Omega)$ are given by Dyson equations:

$$G(\mathbf{k}, i\omega) = \frac{1}{i\omega + \mu - \varepsilon(\mathbf{k}) - \Sigma(\mathbf{k}, i\omega)} \quad (8a)$$

$$W^{\eta}(\mathbf{q}, i\Omega) = \frac{U^{\eta}}{1 - U^{\eta} P^{\eta}(\mathbf{q}, i\Omega)} \quad (8b)$$

$\varepsilon(\mathbf{k})$ is the Fourier transform of t_{ij} ($\varepsilon(\mathbf{k}) = 2t(\cos(k_x) + \cos(k_y)) + 4t'\cos(k_x)\cos(k_y)$), μ the chemical potential, and U^{η} the bare interaction in channel η . In the Heisenberg decoupling^{81,82}:

$$U^{\text{ch}} = (3\alpha - 1)U, \quad U^{\text{sp}} = (\alpha - 2/3)U \quad (9)$$

The ‘‘Fierz parameter’’ α materializes the freedom in choosing the ratio of the charge and spin fluctuations. It reflects the fact (called Fierz ambiguity) that there is no unique way of decoupling the Hubbard interaction with Hubbard-Stratonovich bosons.

The determination of \mathcal{G} and \mathcal{U}^{η} satisfying Eq. (6a-6b) is done by forward recursion (see Suppl. Mat. B).

We have implemented this method and studied it in three physically distinct parameter regimes defined in

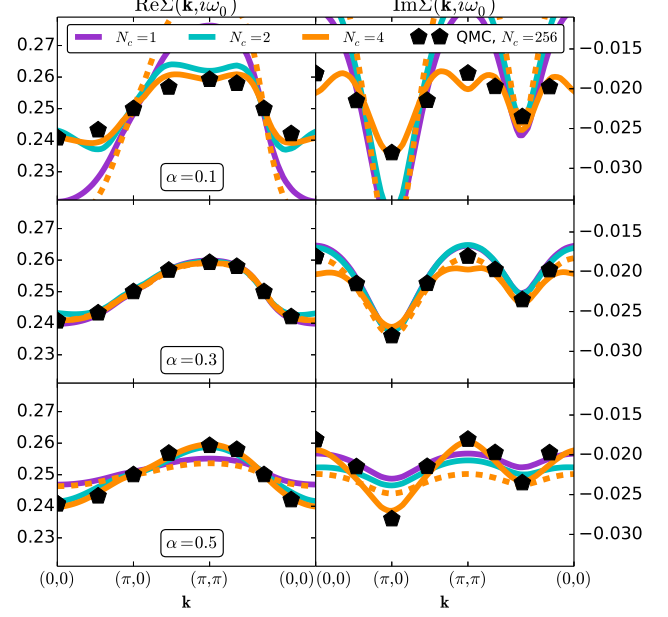


Figure 3. Point A ($U/D = 0.5$, $\delta = 0\%$, $\beta D = 16$, $t' = 0$). $\text{Re}\Sigma(\mathbf{k}, i\omega_0)$ (left column) and $\text{Im}\Sigma(\mathbf{k}, i\omega_0)$ (right column) for $N_c = 1, 2, 4$ for various values of α (from top to bottom), along the path $(0,0) - (\pi,0) - (\pi,\pi) - (0,0)$. Solid lines: TRILEX. Dashed lines: $GW + EDMFT$ ($N_c = 4$). Pentagons: determinant QMC ($N_c = 256$; only a small subset of \mathbf{K} points is shown for a better visibility).

Fig. 2: (A) Weak-coupling regime ($U/D = 0.5$) at half-filling, (B) Intermediate-coupling regime ($U/D = 1$) at large doping, (C) Strong-coupling regime ($U/D = 1.4$) at small doping (the Mott transition occurs at $U_c/D \approx 1.5$ within plaquette cellular DMFT⁸⁴). At these temperatures ($\beta D = 16$ or 8), interaction strengths and dopings, determinant quantum Monte Carlo (QMC) and/or DCA can be converged with respect to N_c . One can thus reach the exact solution of the Hubbard model at these points, albeit at a significant numerical cost. In the following, we compare the cluster TRILEX results obtained with much smaller clusters to these exact benchmarks.

We start with point A. In Fig. 3, we show the self-energy $\Sigma(\mathbf{k}, i\omega_0)$ for cluster sizes of $N_c = 1$ (single-site), 2 (dimer) and 4 (plaquette) and for three different values of α (illustrated in Fig. 2). As N_c increases, the dependence on α becomes milder and milder. At $N_c = 4$, the self-energy is almost independent on α . This can be explained as follows: in the absence of any truncation, the Hubbard-Stratonovich transformations by which the interaction term is decoupled with auxiliary bosonic modes should all yield the same result. In particular, the exact solution will be independent on α . Since, however, one performs the TRILEX approximation of a cluster-local vertex, one *a priori* breaks this

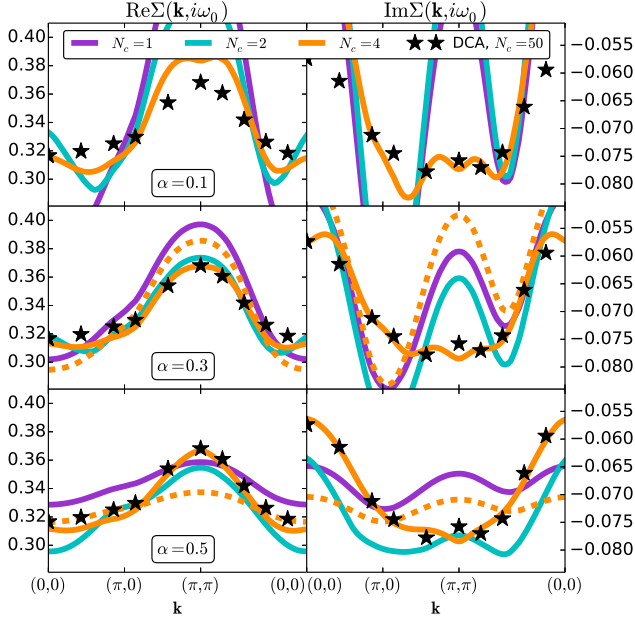


Figure 4. Point B ($U/D = 1$, $\delta = 20\%$, $\beta D = 16$, $t' = 0$). Same conventions as Fig. 3. Stars: DCA from Ref. 55, $N_c = 50$.

equivalence property. As one increases N_c , *i.e.* as one relaxes the locality assumption, one expects that the difference between the curves obtained for different values of α becomes milder.

A first observation is that in this regime, there is an “optimal” value of α ($\alpha = 0.3$) where the results are independent of N_c , at least for the cluster sizes studied here. This shows that when spin fluctuations physics (for $\alpha = 0.3$, $U^{\text{ch}} \approx 0$) is a good phenomenological description (as expected at low U), there is an optimal decoupling where the exact physics is recovered even at the single-site level.

Next, we compare our results with exact determinant QMC⁸⁵ results corresponding to $N_c = 16 \times 16$ sites. The agreement between the exact results and the cluster TRILEX results at $N_c = 4$ is very good both for the real and imaginary parts of the self-energy.

Finally, we compare our results with the self-energy obtained by the $GW + \text{EDMFT}$ method for $N_c = 4$. $GW + \text{EDMFT}$ can be regarded as a simplification of TRILEX with two further approximations to the non-local self-energy contribution: (i) a neglect of the frequency dependence of the vertex (justified in the weak-interaction limit) and (ii) a neglect of the intra-cluster spatial dependence of the vertex. The results obtained with $GW + \text{EDMFT}$ (with $N_c = 4$) can be explained in this light. They are, independently of α , quite close to the single-site TRILEX results (indeed, they are close to a single-site approximation (ii), and the frequency dependence of the vertex is somewhat weak in the low- U

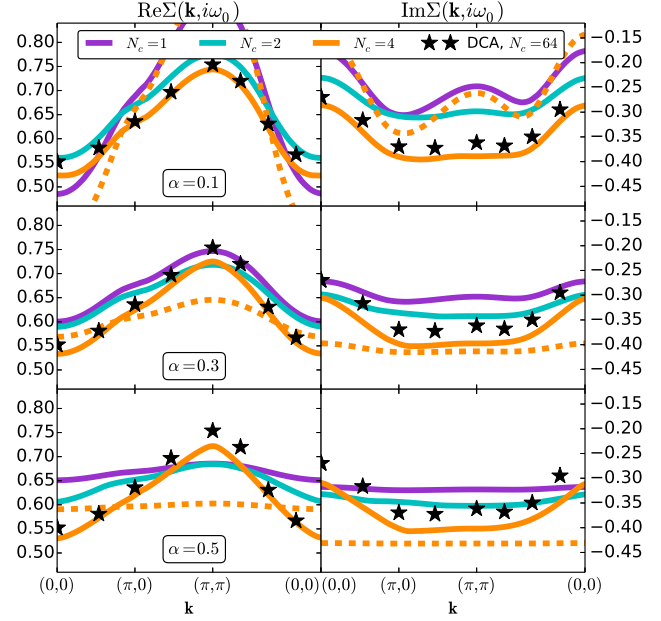


Figure 5. Point C ($U/D = 1.4$, $\delta = 4\%$, $\beta D = 8$, $t'/t = -0.3$). Same conventions as Fig. 3. Stars: DCA, $N_c = 64$.

limit (i)). Second, they are different from the cluster TRILEX results and from the exact solution, except for the optimal value of α ($\alpha = 0.3$) where both methods give results close to the exact solution.

At point B (Fig. 4), the agreement between the converged (DCA) results and the real and imaginary parts of the self-energy, for all values of α (with more important deviations for $\alpha = 0.1$), is very good for $N_c = 4$. Contrary to the weak-coupling limit, no value of α in the single-site case matches the exact solution. This points to the importance of nonlocal corrections to the three-leg vertex. This observation is further corroborated by looking at the $GW + \text{EDMFT}$ curve. There, the agreement with the exact result is quite poor, while being similar to the single-site result, like in the weak-coupling limit (for $\alpha = 0.1$, a spin instability precludes convergence of $GW + \text{EDMFT}$). This discrepancy shows that as interactions are increased, the frequency and momentum dependence of the vertex play a more and more important role in the nonlocal self-energy, as we will discuss below. These conclusions are also valid for local observables (see Suppl. Mat. D).

At strong-coupling point C (Fig. 5), similarly to the previous regimes, the $N_c = 4$ self-energy is almost independent of the Fierz parameter α , and in good agreement with the converged (DCA) solution (especially so for its real part). $GW + \text{EDMFT}$ at $N_c = 4$ is quite far from the exact result, as can be expected from the previous discussion.

Finally, we analyze the momentum and frequency de-

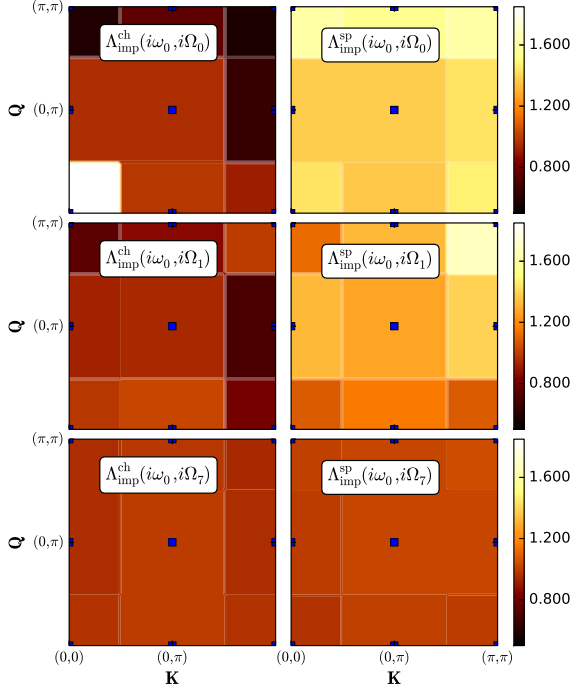


Figure 6. Point B ($U/D = 1$, $\delta = 20\%$, $\beta D = 16$, $t' = 0$), $\alpha = 0.5$. Impurity vertex $\Lambda_{\text{imp}}^{\eta}(\mathbf{K}, \mathbf{Q}; i\omega_0, i\Omega)$ at $\mathbf{K}, \mathbf{Q} \in [(0,0), (0,\pi), (\pi,\pi)]^2$ (the value is color-coded in the square area surrounding each blue point) in the charge (left column) and spin (right column) channels, for increasing bosonic Matsubara frequency (from top to bottom).

pendence of the vertex. It is illustrated in Fig. 6, which represents the \mathbf{K}, \mathbf{Q} dependence of Λ_{imp} at point B. At low energies, the vertex acquires a momentum dependence (especially in the charge channel), while it is essentially local at high energies. In other words, the largest deviations to locality occur at small Matsubara frequencies only (see also Suppl. Mat E). The nonlocal components are smaller or much smaller than the local component, especially for large Matsubara frequencies. This gives an *a posteriori* explanation of the qualitatively good results of the single-site TRILEX approximation. More importantly, the fact that the momentum dependence is confined to low energies suggests possible improvements for the parametrization and computation of the vertex.

In conclusion, we have presented a first implementation of the cluster extension of the TRILEX method, based on the momentum coarse-graining of the three-leg vertex function. For a broad interaction and doping range of the two-dimensional Hubbard model, we obtain, for an embedded cluster with only four impurity sites, continuous self-energies in close agreement with the exact result obtained with comparatively expensive large-cluster lattice QMC and DCA calculations.

We have shown that the Fierz parameter α can be turned into a practical advantage in two ways: First and foremost, we have shown that proximity to the exact solution coincides with stability with respect to α . With this necessary condition, one can assess, at a given (possibly small) cluster size, the accuracy of the solution. Second, in some regimes, there exists an optimal value of α for which accurate results can be reached for smaller cluster sizes (even $N_c = 1$).

This Fierz convergence criterion, along with the relatively small cost of the method, paves the way to a controlled exploration of low-temperature phases such as the superconducting phase of the Hubbard model, where cluster DMFT methods cannot be converged in practice.

ACKNOWLEDGMENTS

We acknowledge useful discussions with M. Ferrero and A. Georges. We especially thank W. Wu for providing us determinant QMC numerical data for the benchmark results of point A and DCA data for point C, as well as J. LeBlanc for providing us the DCA data (from Ref. 55) for point B. This work is supported by the FP7/ERC, under Grant Agreement No. 278472-MottMetals. Part of this work was performed using HPC resources from GENCI-TGCC (Grant No. 2016-t2016056112). Our implementation is based on the TRIQS toolbox⁸⁶.

Supplemental Material A: Fourier conventions and patching details

1. Spatial Fourier transforms

\mathbf{K} and \mathbf{Q} are cluster momenta.

a. Direct transforms

We define:

$$f_{\mathbf{K}} \equiv \frac{1}{N_c} \sum_{ij} e^{-i\mathbf{K}(\mathbf{R}_i - \mathbf{R}_j)} f_{ij} \quad (\text{A1})$$

$$g_{\mathbf{K},\mathbf{Q}} \equiv \frac{1}{N_c} \sum_{ijk} e^{-i\mathbf{K}(\mathbf{R}_i - \mathbf{R}_j) - i\mathbf{Q}(\mathbf{R}_k - \mathbf{R}_j)} g_{ijk} \quad (\text{A2})$$

b. Reciprocal transforms

We define:

$$\begin{aligned} f_{ij} &= \sum_{\mathbf{K}} e^{i\mathbf{K} \cdot (\mathbf{R}_i - \mathbf{R}_j)} f_{\mathbf{K}} \\ g_{ijk} &= \sum_{\mathbf{K}\mathbf{Q}} e^{i\mathbf{K}(\mathbf{R}_i - \mathbf{R}_j) + i\mathbf{Q}(\mathbf{R}_k - \mathbf{R}_j)} g_{\mathbf{K},\mathbf{Q}} \end{aligned}$$

where $\sum_{\mathbf{K}} f_{\mathbf{K}}$ is shorthand for $\frac{1}{N_c} \sum_{i=1}^{N_c} f_{\mathbf{K}_i}$.

2. Temporal Fourier transforms

$i\omega$ (resp. $i\Omega$) denotes fermionic (resp. bosonic) Matsubara frequencies, and are shorthand for $i\omega_n = \frac{2n+1}{\beta}\pi$ (resp. $i\Omega_m = \frac{2m}{\beta}\pi$).

a. Direct transforms

We define:

$$f_{i\omega} \equiv \int_0^{\beta} d\tau e^{i\omega\tau} f_{\tau} \quad (\text{A3})$$

$$g_{i\omega,i\Omega} \equiv \iint_0^{\beta} d\tau d\tau' e^{i\omega\tau + i\Omega\tau'} g_{\tau,\tau'} \quad (\text{A4})$$

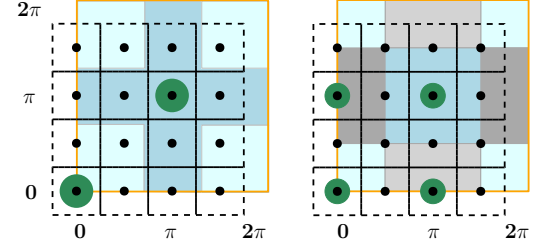


Figure S.1. Example of discretization of the Brillouin zone with $n_{\mathbf{k}} \times n_{\mathbf{k}}$ \mathbf{k} points (here $n_{\mathbf{k}} = 4$) for $N_c = 2$ (left panel) and $N_c = 4$ (right panel)

b. Reciprocal transforms

We define:

$$\begin{aligned} f_{\tau} &= \sum_{i\omega} e^{i\omega\tau} f_{\tau} \\ g_{\tau,\tau'} &= \sum_{i\omega} \sum_{i\Omega} e^{-i\omega\tau - i\Omega\tau'} g_{i\omega,i\Omega} \end{aligned}$$

Here, $\sum_{i\omega} f(i\omega)$ is shorthand for $\frac{1}{\beta} \sum_{n=-n_{\max}}^{n_{\max}-1} f(i\omega_n)$.

3. Patching and discretization

In DCA, the \mathbf{k} integrals can be replaced with integrals on the density of states, e.g.

$$\begin{aligned} G_{\mathbf{K}}(i\omega) &= \sum_{\mathbf{k} \in \mathcal{P}_{\mathbf{K}}} \frac{1}{i\omega + \mu - \varepsilon_{\mathbf{k}} - \Sigma_{\text{imp}}(\mathbf{K}, i\omega)} \\ &= \int_{-\infty}^{\infty} d\varepsilon \frac{D_{\mathbf{K}}(\varepsilon)}{i\omega + \mu - \varepsilon - \Sigma_{\text{imp}}(\mathbf{K}, i\omega)} \end{aligned}$$

where $D_{\mathbf{K}}(\varepsilon) \equiv \sum_{\mathbf{k} \in \mathcal{P}_{\mathbf{K}}} \delta(\varepsilon - \varepsilon_{\mathbf{k}})$ is the noninteracting density of states of patch \mathbf{K} , and where the number of \mathbf{k} points in the computation of the density of states can virtually be pushed to infinity.

By contrast, in cluster TRILEX, the self-energy is a function of \mathbf{k} instead of \mathbf{K} , forbidding this substitution and keeping the number of \mathbf{k} points finite (but large due to the low cost of the computation of $\Sigma(\mathbf{k}, i\omega)$: we typically discretize the Brillouin zone in $n_{\mathbf{k}} \times n_{\mathbf{k}}$ points, with $n_{\mathbf{k}} = 32$).

This requires extra care when defining the theta functions $\theta_{\mathbf{K}}(\mathbf{k})$ defined in a loose way in the main text. $\theta_{\mathbf{K}}(\mathbf{k})$ is precisely defined as the overlap of the area surrounding a given \mathbf{k} point with the patch $\mathcal{P}_{\mathbf{K}}$, divided by the total area surrounding the \mathbf{k} point. This area is illustrated in Fig. S.1 for the case $n_{\mathbf{k}} = 4$. For instance, the \mathbf{k} point of coordinates $(1, 1)$ has $\theta_{\mathbf{K}=(0,0)}(\mathbf{k}) = 1/4$, while that of coordinates $(1, 2)$ has $\theta_{\mathbf{K}=(0,\pi)}(\mathbf{k}) = 1/2$.

Correspondingly, $\sum_{\mathbf{k} \in \mathcal{P}_{\mathbf{K}}}$ is precisely defined as

$$f_{\mathbf{K}} = \sum_{\mathbf{k} \in \mathcal{P}_{\mathbf{K}}} f_{\mathbf{k}} = \frac{\sum_{i=1}^{n_{\mathbf{k}} \times n_{\mathbf{k}}} f(\mathbf{k}_i) \theta_{\mathbf{K}}(\mathbf{k}_i)}{\sum_{i=1}^{n_{\mathbf{k}} \times n_{\mathbf{k}}} \theta_{\mathbf{K}}(\mathbf{k}_i)} \quad (\text{A5})$$

Supplemental Material B: Cluster Trilex Loop

As in Refs 81–83, we solve the cluster TRILEX equations by forward recursion, with the following steps (illustrated in Fig. S.2):

1. Start with a guess $\Sigma(\mathbf{k}, i\omega)$, $P^{\eta}(\mathbf{q}, i\Omega)$
 2. Compute $G(\mathbf{k}, i\omega)$ and $W^{\eta}(\mathbf{q}, i\Omega)$ (Eqs (8)) and then $G(\mathbf{K}, i\omega)$ and $W^{\eta}(\mathbf{Q}, i\Omega)$ (Eqs. (7))
 3. Compute $\mathcal{G}(\mathbf{K}, i\omega)$ and $\mathcal{U}^{\eta}(\mathbf{Q}, i\Omega)$ by substituting Eqs (6) into the impurity Dyson equations, i.e.
- $$\mathcal{G}(\mathbf{K}, i\omega) = [G_{\mathbf{K}}^{-1}(i\omega) + \Sigma_{\text{imp}}(\mathbf{K}, i\omega)]^{-1} \quad (\text{B1a})$$
- $$\mathcal{U}^{\eta}(\mathbf{Q}, i\Omega) = \left[[W_{\mathbf{Q}}^{\eta}]^{-1}(i\Omega) + P_{\text{imp}}^{\eta}(\mathbf{Q}, i\Omega) \right]^{-1} \quad (\text{B1b})$$
4. Solve the impurity model, Eq. (2), for its exact vertex $\Lambda_{\text{imp}}^{\eta}(\mathbf{K}, \mathbf{Q}; i\omega, i\Omega)$ (see Section C for more details).
 5. Compute $\Sigma(\mathbf{k}, i\omega)$ and $P^{\eta}(\mathbf{q}, i\Omega)$ (Eqs (5))
 6. Go back to step 2 until convergence of Σ and P^{η} .

As in Refs 81 and 83, and as justified in Ref. 82 for the single-site impurity case, in the equations presented in the main text and in the loop presented above, we have implicitly approximated the impurity's electron-boson vertex with the bare electron-boson vertex or, in other words, we have assumed the ζ function, introduced in Ref. 82, to be negligible.

Supplemental Material C: Solution of the Impurity Model

1. Impurity solver

The impurity model, defined by Eq. (2), is solved using a continuous-time quantum Monte-Carlo algorithm⁸⁷. Contrary to the single-site case, the densities n_i^I are no longer good quantum numbers due to the intra-cluster hopping terms. This precludes the use of the hybridization expansion algorithms, which can be used with retarded interactions only if the operators involved in the retarded interactions are good quantum numbers, and in which only correlators between operators which are

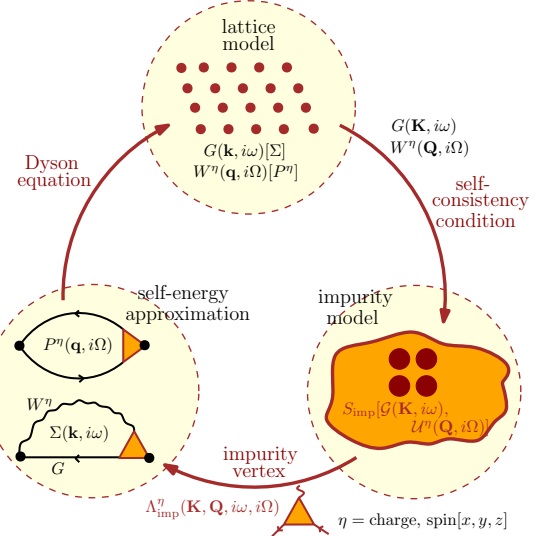


Figure S.2. The cluster TRILEX loop

good quantum numbers can be easily measured. We therefore use an interaction-expansion (CT-INT) algorithm, described *e.g.* in Ref. 88. Here, for the measurement of the three-point function $\tilde{\chi}_{\text{imp}}^{3,\sigma\sigma'}(i, j, k; \tau, \tau')$ (defined in Eq. (C5) below), we use a straightforward operator-insertion method.

We observe that in all the parameter regimes studied in the main text (points A, B and C), the interactions $U_{ij}^I(\tau)$ are static and local to a very good approximation:

$$U_{ij}^I(\tau) \approx U^I \delta_{ij} \delta_{\tau} \quad (\text{C1})$$

This is illustrated in Fig. S.3 for point B. Thus, in practice, we do not have to use the retarded interactions. This simplifies the numerical computation since the dependence of the Monte-Carlo sign problem on CT-INT's density-shifting parameter $\alpha_{\sigma}(s)$ (see *e.g.* Eq. (145) of Ref. 88) is less simple than in the case of static interactions.

2. Computation of $G_{\text{imp}}(\mathbf{K}, i\omega)$ and $W_{\text{imp}}(\mathbf{Q}, i\Omega)$

$G_{\text{imp}}(\mathbf{K}, i\omega)$ and $W_{\text{imp}}(\mathbf{Q}, i\Omega)$ are obtained by computing the spatial and temporal Fourier transforms (defined in Section A) $G_{\text{imp}}(\mathbf{K}, i\omega)$ and $\chi_{\text{imp}}^{\sigma\sigma'}(\mathbf{Q}, i\Omega)$ of the impurity's Green's function and density-density response functions:

$$G_{\text{imp}}(i, j; \tau) \equiv -\langle T c_i(\tau) c_j^{\dagger}(0) \rangle_{\text{imp}} \quad (\text{C2a})$$

$$\chi_{\text{imp}}^{\sigma\sigma'}(i, j; \tau) \equiv \langle T n_{i\sigma}(\tau) n_{j\sigma'}(0) \rangle_{\text{imp}} \quad (\text{C2b})$$

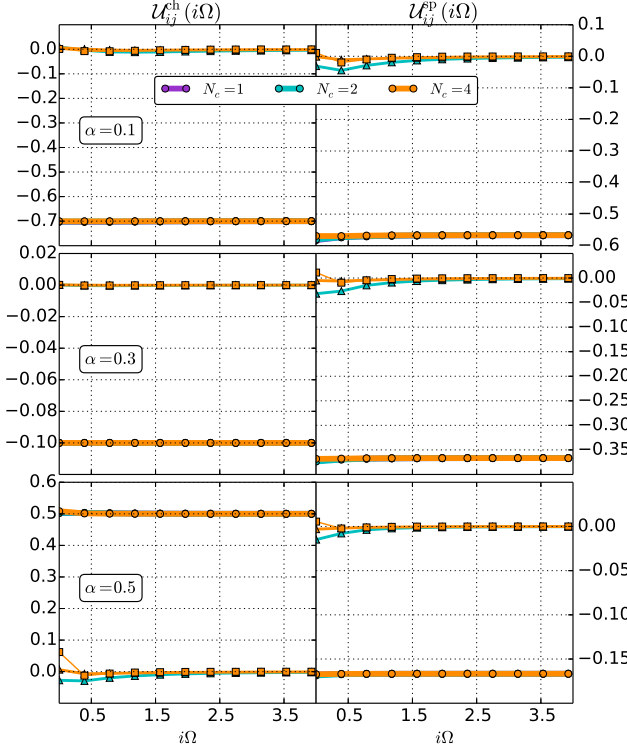


Figure S.3. Retarded interaction $\mathcal{U}_{ij}^\eta(i\Omega)$ in the charge (left column) and spin (right column) channels, for $\alpha = 0.1$ (top row), 0.3 (middle row), 0.5 (bottom row), at point B (see Fig. 2 for a definition). Dots: local component ($i, j = 0, 0$). Triangles: nearest-neighbor component ($i, j = 0, 1$, for $N_c = 2$ and $N_c = 4$ only). Squares: next-nearest-neighbor component ($i, j = 0, 3$, for $N_c = 4$ only).

and by using the identity

$$\begin{aligned} W_{\text{imp}}^\eta(\mathbf{Q}, i\Omega) &= \quad (C3) \\ \mathcal{U}^\eta(\mathbf{Q}, i\Omega) - \mathcal{U}^\eta(\mathbf{Q}, i\Omega)\chi_{\text{imp}}^\eta(\mathbf{Q}, i\Omega)\mathcal{U}^\eta(\mathbf{Q}, i\Omega) \end{aligned}$$

where the passage from spin (σ, σ') to channel (η) indices is done using the expressions:

$$\chi_{\text{imp}}^{\eta=\text{ch}} \equiv \chi_{\text{imp}}^{\uparrow\uparrow} + \chi_{\text{imp}}^{\uparrow\downarrow} \quad (C4a)$$

$$\chi_{\text{imp}}^{\eta=\text{sp}} \equiv \chi_{\text{imp}}^{\uparrow\uparrow} - \chi_{\text{imp}}^{\uparrow\downarrow} \quad (C4b)$$

3. Computation of the cluster vertex

$$\Lambda_{\text{imp}}^\eta(\mathbf{K}, \mathbf{Q}; i\omega, i\Omega)$$

The computation of $\Lambda_{\text{imp}}^\eta(\mathbf{K}, \mathbf{Q}; i\omega, i\Omega)$ is done by measuring the three-point function

$$\tilde{\chi}_{\text{imp}}^{3,\sigma,\sigma'}(i, j, k; \tau, \tau') \equiv \langle T c_{i\sigma}(\tau) c_{j\sigma}^\dagger(0) n_{k\sigma'}(\tau') \rangle_{\text{imp}} \quad (C5)$$

The vertex, written in cluster coordinates $\mathbf{R}_i, \mathbf{R}_j, \mathbf{R}_k$, is then computed as:

$$\begin{aligned} \Lambda_{ijk}^\eta(i\omega, i\Omega) &\equiv \sum_{pqr} G_{\text{imp}}^{-1}(p, j; i\omega + i\Omega) G_{\text{imp}}^{-1}(i, q; i\omega) \\ &\times [1 - \mathcal{U}^\eta \chi_{\text{imp}}^\eta]_{kr}^{-1}(i\Omega) \tilde{\chi}_{\text{imp}}^{3,\eta,\text{conn}}(q, p, r; i\omega, i\Omega) \end{aligned} \quad (C6)$$

with the expression in the charge and spin channel:

$$\tilde{\chi}_{\text{imp}}^{3,\eta=\text{ch}} \equiv \tilde{\chi}_{\text{imp}}^{3,\uparrow\uparrow} + \tilde{\chi}_{\text{imp}}^{3,\uparrow\downarrow} \quad (C7a)$$

$$\tilde{\chi}_{\text{imp}}^{3,\eta=\text{sp}} \equiv \tilde{\chi}_{\text{imp}}^{3,\uparrow\uparrow} - \tilde{\chi}_{\text{imp}}^{3,\uparrow\downarrow} \quad (C7b)$$

and the connected component defined as:

$$\begin{aligned} \tilde{\chi}_{\text{imp}}^{3,\eta,\text{conn}}(i, j, k; i\omega, i\Omega) &\equiv \quad (C8) \\ \tilde{\chi}_{\text{imp}}^{3,\eta}(i, j, k; i\omega, i\Omega) + G_{\text{imp}}(i, j; i\omega) n_k^\eta \delta_{i\Omega} \end{aligned}$$

$\Lambda_{ijk}^\eta(i\omega, i\Omega)$ is then Fourier-transformed to $\Lambda_{\text{imp}}^\eta(\mathbf{K}, \mathbf{Q}; i\omega, i\Omega)$ (see Section A, Eq. (A2)).

In practice, instead of directly performing a temporal Fourier transform to compute $\tilde{\chi}_{\text{imp}}^{3,\sigma\sigma'}(i, j, k; i\omega, i\Omega)$ from $\tilde{\chi}_{\text{imp}}^{3,\sigma\sigma'}(i, j, k; \tau, \tau')$, we first compute the connected component $\tilde{\chi}_{\text{imp}}^{3,\eta,\text{conn}}(i, j, k; \tau, \tau')$ (defined in Eq. (C8), which is smooth and without discontinuities, perform a cubic spline interpolation of it, and then Fourier transform it to Matsubara frequencies. This allows us to use a small number (typically $n_\tau = 100$) of τ, τ' points in the measurement.

Supplemental Material D: Self-energy

1. Self-energy decomposition

In this section, we show that the coarse-grainings introduced for the vertex allow for a numerically convenient decomposition of Σ and P .

Following a procedure very similar to that described in section II.D.3 of Ref. 82, we decompose Eqs (5) as follows:

$$\Sigma(\mathbf{k}, i\omega) = \Sigma_{\text{imp}}(i, j = 0, 0; i\omega) \quad (D1a)$$

$$- \sum_\eta m_\eta \sum_{\mathbf{K}, \mathbf{Q}} \sum_{\mathbf{q}, i\omega} \tilde{G}_{\mathbf{k}+\mathbf{q}, i\omega+i\Omega}^{\mathbf{K}+\mathbf{Q}} \tilde{W}_{\mathbf{q}, i\omega}^{\eta, \mathbf{Q}} \Lambda_{\text{imp}}^\eta(\mathbf{K}, \mathbf{Q}; i\omega, i\Omega)$$

$$P^\eta(\mathbf{q}, i\Omega) = P_{\text{imp}}^\eta(i, j = 0, 0; i\Omega) \quad (D1b)$$

$$+ 2 \sum_{\mathbf{K}, \mathbf{Q}} \sum_{\mathbf{k}, i\omega} \tilde{G}_{\mathbf{k}+\mathbf{q}, i\omega+i\Omega}^{\mathbf{K}+\mathbf{Q}} \tilde{G}_{\mathbf{k}, i\omega}^{\mathbf{K}} \Lambda_{\text{imp}}^\eta(\mathbf{K}, \mathbf{Q}; i\omega, i\Omega)$$

where we have defined the nonlocal components:

$$\tilde{X}(\mathbf{k}, i\omega) \equiv X(\mathbf{k}, i\omega) - \sum_{\mathbf{k}'} X(\mathbf{k}, i\omega) \quad (\text{D2})$$

Indeed, decomposing Eq. (5a) using Eq. (D2), and expanding, one obtains four terms, two of which vanish. The two remaining terms are given in Eq. (D1a). The first term is given by $\Sigma_{\text{imp}}(00, i\omega)$:

$$\begin{aligned} & - \sum_{\eta} m_{\eta} \sum_{\mathbf{K}, \mathbf{Q}} \sum_{i\Omega} \left\{ \sum_{\mathbf{k}'} G_{i\omega+i\Omega}(\mathbf{k}') \theta_{\mathbf{K}+\mathbf{Q}}(\mathbf{k}') \right\} \\ & \times \left\{ \sum_{\mathbf{q}'} W_{i\Omega}(\mathbf{q}') \theta_{\mathbf{Q}}(\mathbf{q}') \right\} \Lambda_{\text{imp}}^{\eta}(\mathbf{K}, \mathbf{Q}; i\omega, i\Omega) \quad (\text{D3}) \end{aligned}$$

$$\begin{aligned} & = - \sum_{\eta} m_{\eta} \sum_{i\Omega} \sum_{\mathbf{q}'} \sum_{\mathbf{k}'} \{G_{i\omega+i\Omega}(\mathbf{k}' + \mathbf{q}')\} \{W_{i\Omega}(\mathbf{q}')\} \\ & \times \sum_{\mathbf{KQ}} \theta_{\mathbf{K}+\mathbf{Q}}(\mathbf{k}' + \mathbf{q}') \theta_{\mathbf{Q}}(\mathbf{q}') \Lambda_{\text{imp}}^{\eta}(\mathbf{K}, \mathbf{Q}; i\omega, i\Omega) \quad (\text{D4}) \end{aligned}$$

$$\begin{aligned} & = - \sum_{\mathbf{k}'} \sum_{\eta} m_{\eta} \sum_{\mathbf{q}'} \sum_{i\Omega} G_{i\omega+i\Omega}(\mathbf{k}' + \mathbf{q}') W_{i\Omega}(\mathbf{q}') \Lambda_{\mathbf{k}', \mathbf{q}'}^{\eta}(i\omega, i\Omega) \\ & = \sum_{\mathbf{k}'} \Sigma(\mathbf{k}', i\omega) \\ & = \Sigma(\mathbf{R} = 0, i\omega) \\ & = \Sigma_{\text{imp}}(0, 0; i\omega) \quad (\text{D5}) \end{aligned}$$

A similar result holds for P .

In the second terms of Eqs (D1a-D1b), the summands decay fast for large Matsubara frequencies thanks to the fast decay of the nonlocal component $\tilde{G}(\mathbf{k}, i\omega)$ and $\tilde{W}(\mathbf{q}, i\Omega)$.

As in Ref. 82, we furthermore split Λ into a “regular part” $\Lambda^{\eta, \text{reg}}$ which vanishes at large frequencies

$$\Lambda_{ijk}^{\eta, \text{reg}}(i\omega, i\Omega) = \Lambda_{ijk}^{\eta}(i\omega, i\Omega) - l_{ijk}(i\Omega) \quad (\text{D6})$$

and a remainder $l(i\Omega)$ corresponding to the high-frequency asymptotics of the three-point function:

$$l_{ijk}(i\Omega) \equiv \sum_p [1 - \mathcal{U}^{\eta} \chi^{\eta}]_{kp}^{-1}(i\Omega) \delta_{ij} \quad (\text{D7})$$

The term containing $\Lambda_{ijk}^{\eta, \text{reg}}(i\omega, i\Omega)$ has a quickly decaying summand thanks to \tilde{G} , \tilde{W} and Λ^{reg} . We compute it in Matsubara frequencies and real space after a fast Fourier transform of \tilde{G} and \tilde{W} . This is the bottleneck of the computation of the self-energy as it scales as $O(N_{\omega}^2 N_k \log N_k N_c^2)$ (where N_{ω} is the number of Matsubara frequencies used and N_k the number of \mathbf{k} points in the discretized first Brillouin zone). The term containing $l_{ijk}(i\Omega)$ can be computed entirely in imaginary time and real space, with a computational complexity of $O(N_{\omega} \log N_{\omega} N_k \log N_k N_c^2)$.

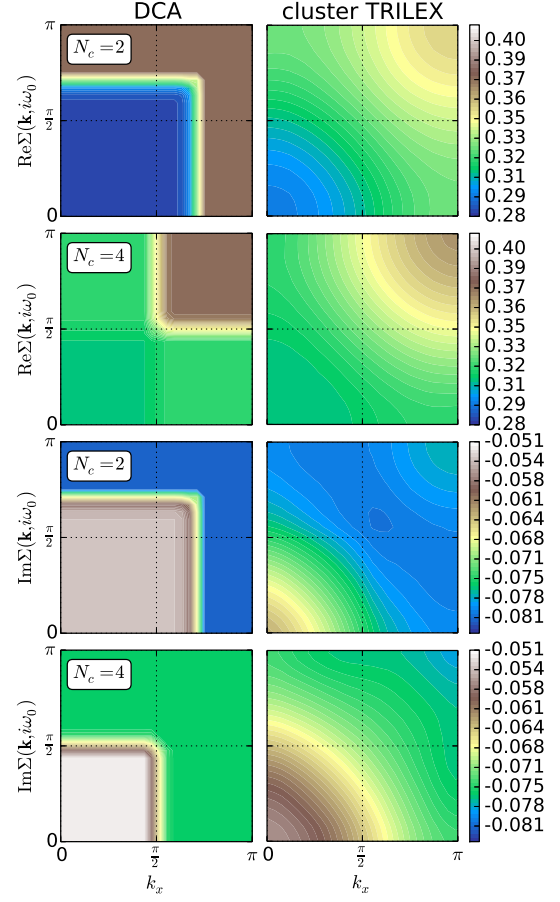


Figure S.4. $\Sigma(\mathbf{k}, i\omega_0)$ in the upper quadrant of the first Brillouin zone, at point B ($U/D = 1$, $\delta = 20\%$, $\beta D = 16$, $t' = 0$). Left column: DCA, right column: cluster TRILEX. First two rows: real part, last two rows: imaginary part. Odd rows: $N_c = 2$, even rows: $N_c = 4$.

2. Continuity of the self-energy

In Fig. S.4, we show the lowest Matsubara component of the self-energy obtained in the dynamical cluster approximation (DCA) and the one obtained within cluster TRILEX, using Eq. (D1a). While the DCA self-energy is piecewise constant in the Brillouin zone (with discontinuities at the patch edges), the cluster TRILEX self-energy is continuous by construction, similarly to what is achieved by the DCA⁺ method^{89,90}, but without arbitrary interpolation schemes.

3. Local components

In Fig. S.5, we display the local components G_{loc} and Σ_{imp} and compare them to benchmark results obtained with DCA ($N_c = 50$, Ref. 55). The $N_c = 4$ cluster

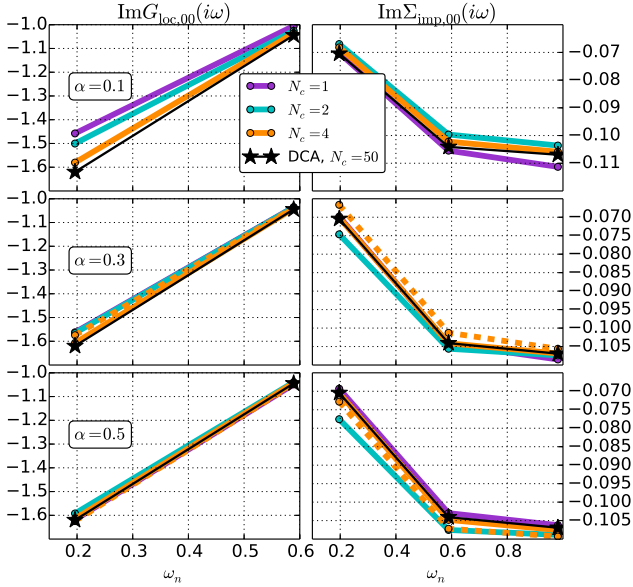


Figure S.5. (Point B: $U/D = 1$, $\delta = 20\%$, $\beta D = 16$, $t' = 0$). Imaginary part of the local components of G_{loc} (left column) and Σ_{imp} (right column) for $\alpha = 0.1$ (top row), 0.3 (middle row), 0.5 (bottom row) and different N_c . Solid lines: TRILEX. Dashed lines: $GW + \text{EDMFT}$ ($N_c = 4$). Black stars: DCA result from Ref. 55, $N_c = 50$.

TRILEX data is the closest to the benchmark data, irrespective of the value of α .

Supplemental Material E: Vertex

1. Momentum dependence of the vertex

In Figures S.6 and S.7, we show the dependence of the vertex on the cluster momenta \mathbf{K} and \mathbf{Q} for points A and C (point B is shown in the main text).

2. Cluster-site dependence of the vertex

In Figures S.8, S.9 and S.10, we show all the inequivalent vertex components $\Lambda_{\text{imp}}(i, j, k; i\omega, i\Omega)$ for the three regimes of parameters (respectively point A, B and C) studied in the main text. While the largest component is the local component ($i, j, k = 0, 0, 0$), some nonlocal components are non-negligible.

- ¹ A. V. Chubukov, D. Pines, and J. Schmalian, in *Superconductivity* (Springer Berlin Heidelberg, Berlin, Heidelberg, 2002) Chap. 22, pp. 1349–1413.
- ² F. Onufrieva and P. Pfeuty, *Physical Review Letters* **102**, 207003 (2009).
- ³ M. A. Metlitski and S. Sachdev, *Physical Review B* **82**, 075128 (2010).
- ⁴ K. B. Efetov, H. Meier, and C. Pépin, *Nature Physics* **9**, 442 (2013).
- ⁵ F. Onufrieva and P. Pfeuty, *Physical Review Letters* **109**, 257001 (2012).
- ⁶ D. J. Scalapino, *Reviews of Modern Physics* **84**, 1383 (2012).
- ⁷ Y. Wang and A. Chubukov, *Physical Review B* **90**, 035149 (2014).
- ⁸ Y. Wang, A. Abanov, B. L. Altshuler, E. A. Yuzbashyan, and A. V. Chubukov, *Physical Review Letters* **117**, 157001 (2016).
- ⁹ N. Bickers and D. Scalapino, *Annals of Physics* **206**, 251, 206 (1989).
- ¹⁰ L. Hedin, *Physical Review* **139**, 796 (1965).
- ¹¹ L. Hedin, *Journal of Physics: Condensed Matter* **489** (1999).
- ¹² G. M. Eliashberg, Sov. Phys. JETP **11**, 696 (1960).
- ¹³ J. Jaeckel and C. Wetterich, *Physical Review D* **68**, 025020 (2003).
- ¹⁴ T. Baier, E. Bick, and C. Wetterich, *Physical Review B* **70**, 125111 (2004).
- ¹⁵ L. Bartosch, H. Freire, J. J. R. Cardenas, and P. Kopietz, *Journal of Physics: Condensed Matter* **21**, 305602 (2009).
- ¹⁶ K. Borejsza and N. Dupuis, *Europhysics Letters (EPL)* **63**, 722 (2003).
- ¹⁷ K. Borejsza and N. Dupuis, *Physical Review B* **69**, 085119 (2004).
- ¹⁸ N. Dupuis, *Physical Review B* **65**, 245118 (2002).
- ¹⁹ P. W. Anderson, *Science* **235**, 1196 (1987).
- ²⁰ A. Georges, G. Kotliar, W. Krauth, and M. J. Rozenberg, *Reviews of Modern Physics* **68**, 13 (1996).
- ²¹ M. H. Hettler, A. N. Tahvildar-Zadeh, M. Jarrell, T. Pruschke, and H. R. Krishnamurthy, *Physical Review B* **58**, R7475 (1998).
- ²² M. H. Hettler, M. Mukherjee, M. Jarrell, and H. R. Krishnamurthy, *Physical Review B* **61**, 12739 (1999).
- ²³ A. I. Lichtenstein and M. I. Katsnelson, *Physical Review B* **62**, R9283 (2000).
- ²⁴ G. Kotliar, S. Savrasov, G. Pálsson, and G. Biroli, *Physical Review Letters* **87**, 186401 (2001).
- ²⁵ T. A. Maier, M. Jarrell, T. Pruschke, and M. H. Hettler, *Reviews of Modern Physics* **77**, 1027 (2005).
- ²⁶ B. Kyung, D. Sénéchal, and A.-M. S. Tremblay, *Physical Review B* **80**, 205109 (2009).
- ²⁷ G. Sordi, P. Sémond, K. Haule, and A.-M. S. Tremblay, *Physical Review Letters* **108**, 216401 (2012).
- ²⁸ M. Civelli, M. Capone, A. Georges, K. Haule, O. Parcollet, T. D. Stanescu, and G. Kotliar, *Physical Review Letters* **100**, 046402 (2008).

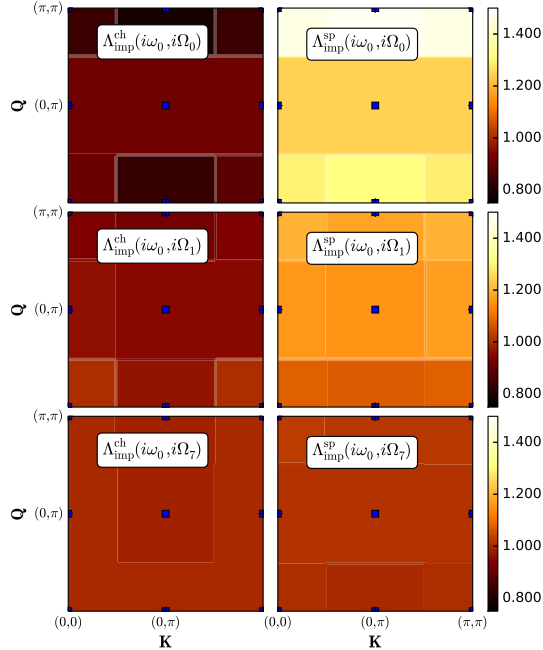


Figure S.6. Weak-coupling parameters (Point A, $U/D = 0.5$, $\delta = 0\%$, $\beta D = 16$, $t' = 0$, $\alpha = 0.5$). Same conventions as Fig. 2.

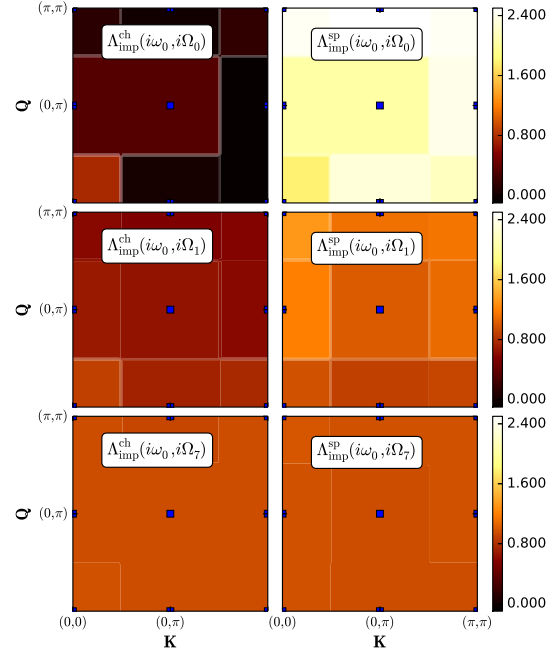


Figure S.7. Strong-coupling parameters (Point C, $U/D = 1.4$, $\delta = 4\%$, $\beta D = 8$, $t'/t = -0.3$, $\alpha = 0.5$). Same conventions as Fig. 2.

- ²⁹ M. Ferrero, O. Parcollet, a. Georges, G. Kotliar, and D. N. Basov, *Physical Review B* **82**, 054502 (2010).
- ³⁰ E. Gull, O. Parcollet, and A. J. Millis, *Physical Review Letters* **110**, 216405 (2013).
- ³¹ A. Macridin, M. Jarrell, and T. A. Maier, *Physical Review B* **70**, 113105 (2004).
- ³² T. A. Maier, M. Jarrell, A. Macridin, and C. Slezak, *Physical Review Letters* **92**, 027005 (2004).
- ³³ T. A. Maier, M. Jarrell, T. C. Schulthess, P. R. C. Kent, and J. B. White, *Physical Review Letters* **95**, 237001 (2005).
- ³⁴ T. Maier, M. Jarrell, and D. Scalapino, *Physical Review Letters* **96**, 047005 (2006).
- ³⁵ E. Gull, M. Ferrero, O. Parcollet, A. Georges, and A. J. Millis, *Physical Review B* **82**, 155101 (2010).
- ³⁶ S. X. Yang, H. Fotso, S. Q. Su, D. Galanakis, E. Khatami, J. H. She, J. Moreno, J. Zaanen, and M. Jarrell, *Physical Review Letters* **106**, 047004 (2011).
- ³⁷ A. Macridin and M. Jarrell, *Physical Review B* **78**, 241101(R) (2008).
- ³⁸ A. Macridin, M. Jarrell, T. Maier, P. R. C. Kent, and E. D'Azevedo, *Physical Review Letters* **97**, 036401 (2006).
- ³⁹ M. Jarrell, T. A. Maier, C. Huscroft, and S. Moukouri, *Physical Review B* **64**, 195130 (2001).
- ⁴⁰ O. Parcollet, G. Biroli, and G. Kotliar, *Physical Review Letters* **92**, 226402 (2004).
- ⁴¹ P. Werner, E. Gull, O. Parcollet, and A. J. Millis, *Physical Review B* **80**, 045120 (2009).
- ⁴² G. Biroli, O. Parcollet, and G. Kotliar, *Physical Review B* **69**, 205108 (2004).
- ⁴³ D. Bergeron, V. Hankevych, B. Kyung, and A.-M. S. Tremblay, *Physical Review B* **84**, 085128 (2011).
- ⁴⁴ B. Kyung, V. Hankevych, A.-M. Daré, and A.-M. Tremblay, *Physical Review Letters* **93**, 147004 (2004).
- ⁴⁵ B. Kyung, S. S. Kancharla, D. Sénéchal, A.-M. S. Tremblay, M. Civelli, and G. Kotliar, *Physical Review B* **73**, 165114 (2006).
- ⁴⁶ S. Okamoto, D. Sénéchal, M. Civelli, and A.-M. S. Tremblay, *Physical Review B* **82**, 180511 (2010).
- ⁴⁷ G. Sordi, K. Haule, and A.-M. S. Tremblay, *Physical Review Letters* **104**, 226402 (2010).
- ⁴⁸ G. Sordi, P. Sémond, K. Haule, and A.-M. S. Tremblay, *Scientific Reports* **2**, 547 (2012).
- ⁴⁹ M. Civelli, M. Capone, S. S. Kancharla, O. Parcollet, and G. Kotliar, *Physical Review Letters* **95**, 106402 (2005).
- ⁵⁰ M. Ferrero, P. S. Cornaglia, L. De Leo, O. Parcollet, G. Kotliar, and A. Georges, *Europhysics Letters* **85**, 57009 (2008).
- ⁵¹ M. Ferrero, P. Cornaglia, L. De Leo, O. Parcollet, G. Kotliar, and A. Georges, *Physical Review B* **80**, 064501 (2009).
- ⁵² E. Gull, O. Parcollet, P. Werner, and A. J. Millis, *Physical Review B* **80**, 245102 (2009).
- ⁵³ X. Chen, J. P. F. LeBlanc, and E. Gull, *Physical Review Letters* **115**, 116402 (2015).
- ⁵⁴ X. Chen, J. P. F. LeBlanc, and E. Gull, *Nature Communications* **8**, 14986 (2017).
- ⁵⁵ J. P. F. LeBlanc, A. E. Antipov, F. Becca, I. W. Bulik, G. K.-L. Chan, C.-M. Chung, Y. Deng, M. Ferrero, T. M. Henderson, C. A. Jiménez-Hoyos, E. Kozik, X.-W. Liu, A. J. Millis, N. V. Prokof'ev, M. Qin, G. E. Scuseria, H. Shi, B. V. Svistunov, L. F. Tocchio, I. S. Tupitsyn,

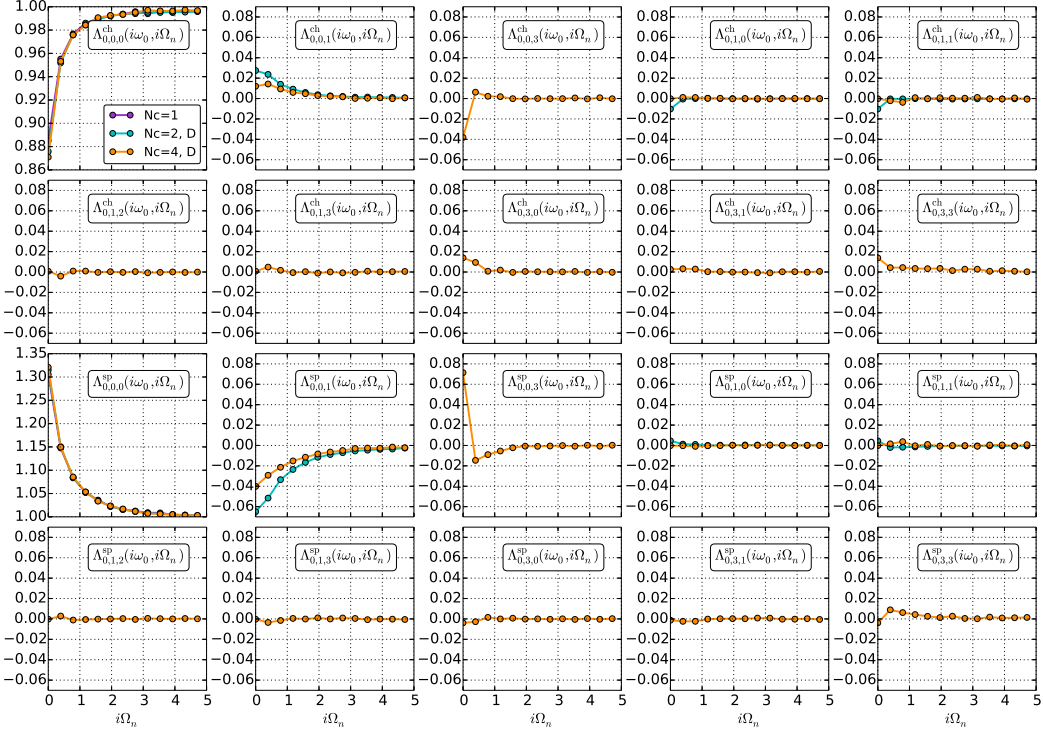


Figure S.8. Weak-coupling parameters (Point A, $U/D = 0.5$, $\delta = 0\%$, $\beta D = 16$, $t' = 0$), $\alpha = 0.5$. Impurity cluster vertex $\Lambda_{\text{imp}}^{\eta}(i, j, k; i\omega, i\Omega)$ in the charge (first two rows) and spin (last two rows) channels, at fixed fermionic Matsubara frequency ω_0 . See Fig 1 for a definition of the cluster coordinates $\mathbf{R}_i, \mathbf{R}_j$ and \mathbf{R}_k denoted by the indices i, j, k .

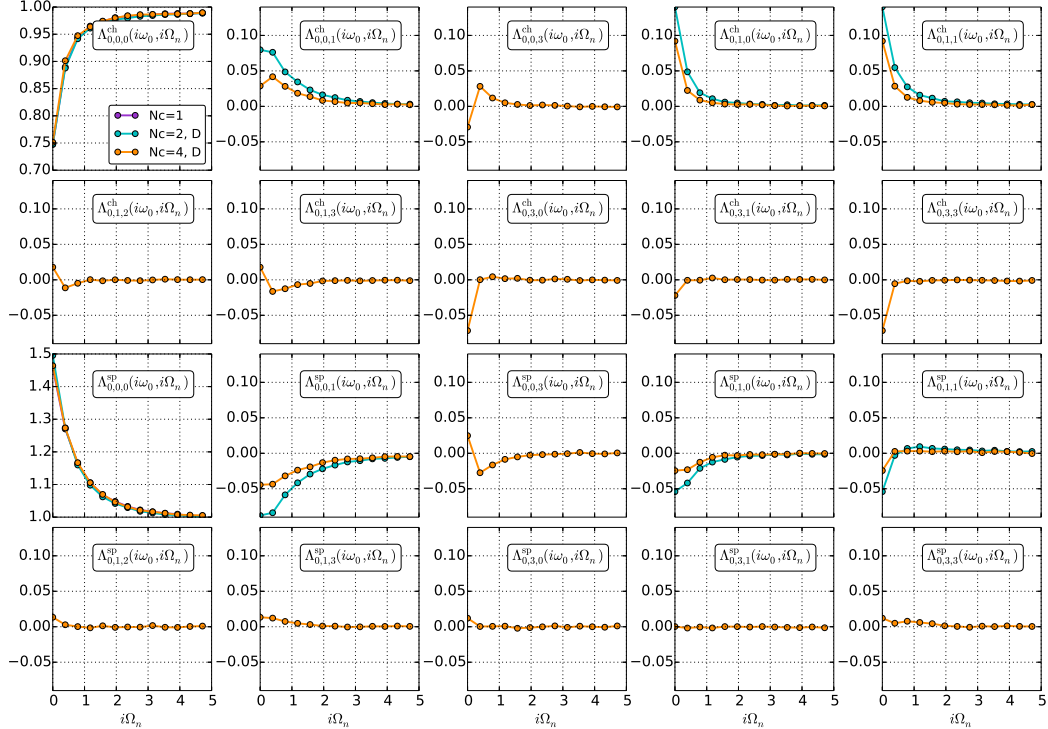


Figure S.9. Intermediate-coupling parameters (point B, $U/D = 1$, $\delta = 20\%$, $\beta D = 16$, $t' = 0$), $\alpha = 0.5$. Impurity cluster vertex $\Lambda_{\text{imp}}^{\eta}(i, j, k; i\omega_0, i\Omega_n)$ in the charge and spin channels, at fixed fermionic Matsubara frequency ω_0 .

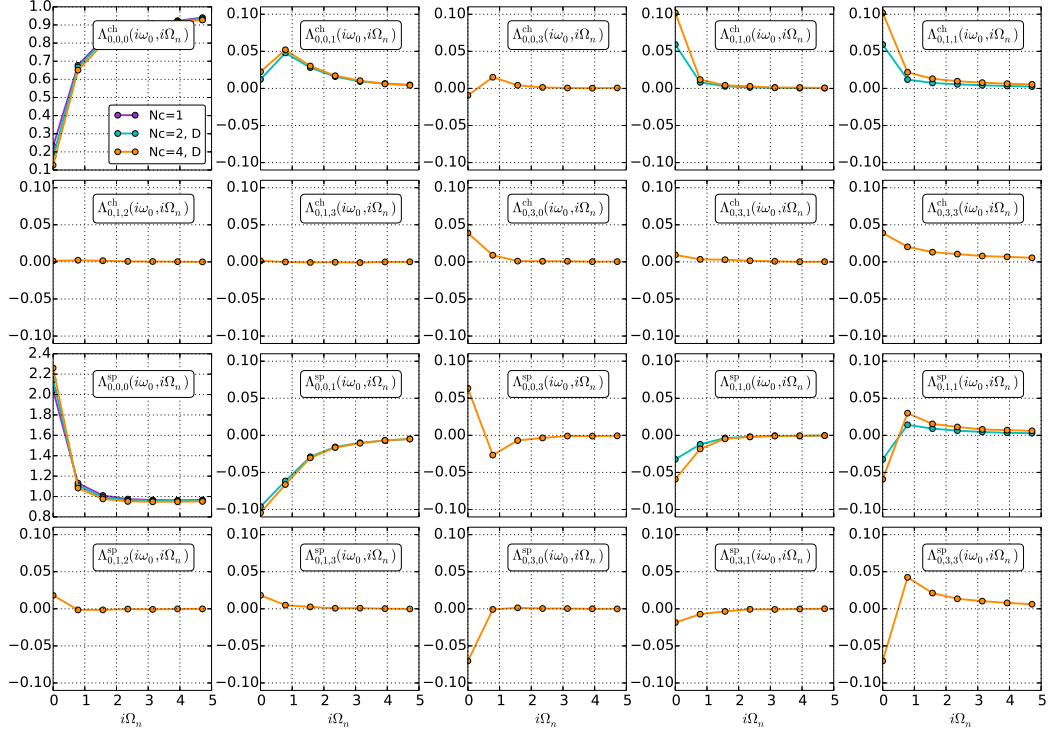


Figure S.10. Strong-coupling parameters (Point C, $U/D = 1.4$, $\delta = 4\%$, $\beta D = 8$, $t'/t = -0.3$, $\alpha = 0.5$). Impurity cluster vertex $\Lambda_{\text{imp}}^\eta(i, j, k; i\omega, i\Omega)$ in the charge and spin channels, at fixed fermionic Matsubara frequency ω_0 .

- S. R. White, S. Zhang, B.-X. Zheng, Z. Zhu, and E. Gull, *Physical Review X* **5**, 041041 (2015).
- ⁵⁶ O. Gunnarsson, T. Schäfer, J. P. F. LeBlanc, E. Gull, J. Merino, G. Sangiovanni, G. Rohringer, and A. Toschi, *Physical Review Letters* **114**, 236402 (2015).
- ⁵⁷ O. Gunnarsson, T. Schäfer, J. P. F. LeBlanc, J. Merino, G. Sangiovanni, G. Rohringer, and A. Toschi, [arXiv:1604.01614](#).
- ⁵⁸ W. Wu, M. Ferrero, A. Georges, and E. Kozik, [arXiv:1608.08402](#).
- ⁵⁹ G. Rohringer, H. Hafermann, A. Toschi, A. A. Katanin, A. E. Antipov, M. I. Katsnelson, A. I. Lichtenstein, A. N. Rubtsov, and K. Held, [arXiv:1705.00024](#).
- ⁶⁰ S. Biermann, F. Aryasetiawan, and A. Georges, *Physical Review Letters* **90**, 086402 (2003).
- ⁶¹ P. Sun and G. Kotliar, *Physical Review B* **66**, 085120 (2002).
- ⁶² P. Sun and G. Kotliar, *Physical Review Letters* **92**, 196402 (2004).
- ⁶³ T. Ayral, P. Werner, and S. Biermann, *Physical Review Letters* **109**, 226401 (2012).
- ⁶⁴ T. Ayral, S. Biermann, and P. Werner, *Physical Review B* **87**, 125149 (2013).
- ⁶⁵ S. Biermann, *Journal of physics. Condensed matter : an Institute of Physics journal* **26**, 173202 (2014).
- ⁶⁶ T. Ayral, S. Biermann, P. Werner, and L. V. Boehnke, [arXiv:1701.07718](#).
- ⁶⁷ A. N. Rubtsov, M. I. Katsnelson, and A. I. Lichtenstein, *Physical Review B* **77**, 033101 (2008).
- ⁶⁸ A. N. Rubtsov, M. I. Katsnelson, and A. I. Lichtenstein, *Annals of Physics* **327**, 1320 (2012).
- ⁶⁹ E. G. C. P. van Loon, A. I. Lichtenstein, M. I. Katsnelson, O. Parcollet, and H. Hafermann, *Physical Review B* **90**, 235135 (2014).
- ⁷⁰ E. A. Stepanov, E. G. C. P. van Loon, A. A. Katanin, A. I. Lichtenstein, M. I. Katsnelson, and A. N. Rubtsov, *Physical Review B* **93**, 045107 (2016).
- ⁷¹ A. Toschi, A. Katanin, and K. Held, *Physical Review B* **75**, 045118 (2007).
- ⁷² A. Katanin, A. Toschi, and K. Held, *Physical Review B* **80**, 075104 (2009).
- ⁷³ T. Schäfer, F. Geles, D. Rost, G. Rohringer, E. Arrigoni, K. Held, N. Blümer, M. Aichhorn, and A. Toschi, *Physical Review B* **91**, 125109 (2015).
- ⁷⁴ A. Valli, T. Schäfer, P. Thunström, G. Rohringer, S. Andergassen, G. Sangiovanni, K. Held, and A. Toschi, *Physical Review B* **91**, 115115 (2015).
- ⁷⁵ G. Li, N. Wentzell, P. Pudleiner, P. Thunström, and K. Held, *Physical Review B* **93**, 165103 (2016).
- ⁷⁶ G. Rohringer and A. Toschi, *Physical Review B* **94**, 125144 (2016).
- ⁷⁷ T. Ayral and O. Parcollet, *Physical Review B* **94**, 075159 (2016).
- ⁷⁸ H. Hafermann, S. Brener, A. N. Rubtsov, M. I. Katsnelson, and A. I. Lichtenstein, *JETP Letters* **86**, 677 (2008).
- ⁷⁹ C. Slezak, M. Jarrell, T. Maier, and J. Deisz, *Journal of Physics: Condensed Matter* **21**, 435604 (2009).
- ⁸⁰ S. X. Yang, H. Fotso, H. Hafermann, K. M. Tam, J. Moreno, T. Pruschke, and M. Jarrell, *Physical Re-*

- view B **84**, 155106 (2011).
- ⁸¹ T. Ayral and O. Parcollet, *Physical Review B* **92**, 115109 (2015).
- ⁸² T. Ayral and O. Parcollet, *Physical Review B* **93**, 235124 (2016).
- ⁸³ J. Vučičević, T. Ayral, and O. Parcollet, [arXiv:1705.08332](https://arxiv.org/abs/1705.08332).
- ⁸⁴ H. Park, K. Haule, and G. Kotliar, *Physical Review Letters* **101**, 186403 (2008).
- ⁸⁵ R. Blankenbecler, D. J. Scalapino, and R. L. Sugar, *Physical Review D* **24**, 2278 (1981).
- ⁸⁶ O. Parcollet, M. Ferrero, T. Ayral, H. Hafermann, P. Seth, and I. S. Krivenko, *Computer Physics Communications* **196**, 398 (2015).
- ⁸⁷ A. N. Rubtsov, V. V. Savkin, and A. I. Lichtenstein, *Physical Review B* **72**, 035122 (2005).
- ⁸⁸ E. Gull, A. J. Millis, A. I. Lichtenstein, A. N. Rubtsov, M. Troyer, and P. Werner, *Reviews of Modern Physics* **83**, 349 (2011).
- ⁸⁹ P. Staar, T. Maier, and T. C. Schulthess, *Physical Review B* **88**, 115101 (2013).
- ⁹⁰ P. Staar, T. Maier, and T. C. Schulthess, *Physical Review B* **89**, 195133 (2014).